nature portfolio

https://doi.org/10.1038/s41561-022-01016-y

Supplementary information

Last Interglacial decadal sea surface temperature variability in the eastern Mediterranean

In the format provided by the authors and unedited

Supplementary material

Last Interglacial decadal sea surface temperature variability in the Eastern Mediterranean

Igor Obreht[1], David De Vleeschouwer[1,2], Lars Wörmer[1], Michal Kucera[1], Devika Varma[1,†], Matthias Prange[1], Thomas Laepple[1,3], Jenny Wendt[1], Sri D. Nandini-Weiss[1,‡], Hartmut Schulz[4], Kai-Uwe Hinrichs[1]

[1]MARUM – Center for Marine Environmental Sciences and Department of Geosciences, University of Bremen, Leobener Str. 8, 28359 Bremen, Germany

[2]Institute of Geology and Paleontology, University of Münster, Corrensstr 24, 48149 Münster, Germany.

[3]Alfred Wegener Institute Helmholtz Centre for Polar and Marine Research, Telegrafenberg A43, 14473 Potsdam, Germany

[4]Fachbereich Geowissenschaften, Eberhard-Karls University, Schnarrenbergstr. 94-96, 72076 Tübingen, Germany

[†]Present address: NIOZ Royal Netherlands Institute for Sea Research, Den Burg, and Utrecht University, Netherlands

[‡]Present address: Institute of Oceanography, Center for Earth System Research and Sustainability (CEN), University of Hamburg, Germany

Supplementary discussion

Lithostratigraphy of M51/3-SL104 core

The studied sediment core M51/3-SL104 was collected from the Eastern Mediterranean during the RV METEOR M51-3 expedition cruise from La Valetta to Istanbul. The core was obtained from the south-east of Crete in the north-western Levantine Sea (location 34.8247°N, 27.2925°E) at a water depth of 2155 m from a part of the Pliny Trench. Sapropel S5 from sediment core M51/3-SL104 is selected from a suite of cores (M40/4-SL67, -KL51; M51/3-SL103, -SL104) all taken from a spot within ~2.5 km on a plateau from the Pliny Trench. The individual ~90 and 85 cm thick sapropels S5 are well correlatable on the basis of internal sedimentary structures, such as layering and lamination, color, element geochemistry, and fossil content[6]. Moreover, a faint ash layer is found at ~4 cm sapropel depth in all 4 cores[8]. Here, we focus our investigation on gravity core M51/3-SL104, where in addition to XRF-element scanning (0.2 mm-spacing) and planktonic foraminiferal counts (continuous 3 mm-spacing), continuous, resin-impregnated thins section have been prepared and quantitatively described[2,6].

The sapropel S5 horizon in the investigated core is dark in colour and it can be clearly separated from the surrounding bright marls (Supplementary Fig. 1). The sapropel spans around 86.8 cm ranging from 359.5-446.3 cm. The sapropel is characterized by a complex lithostratigraphic structure, where a macroscopic layering of alternating mm- to cm-scale darker and brighter beds are visible (first-order lamination). Following the microscopic investigations, the different character of lamination of sapropelic sediment can be divided into (1) a basal, darker-colored section (the lower 9 cm), where for instance the bright-coloured siliceous-rich material is dissolved and (2) an upper, more diatomic regime consisting of dark/bright couplets, representing unbioturbated strictly autochthonous sediment layering. Presumably, it is this extraordinary preservation of silica that is responsible for the thickness of our S5 sapropel, when compared to typical eastern Mediterranean sapropels of 20-40 cm thickness.

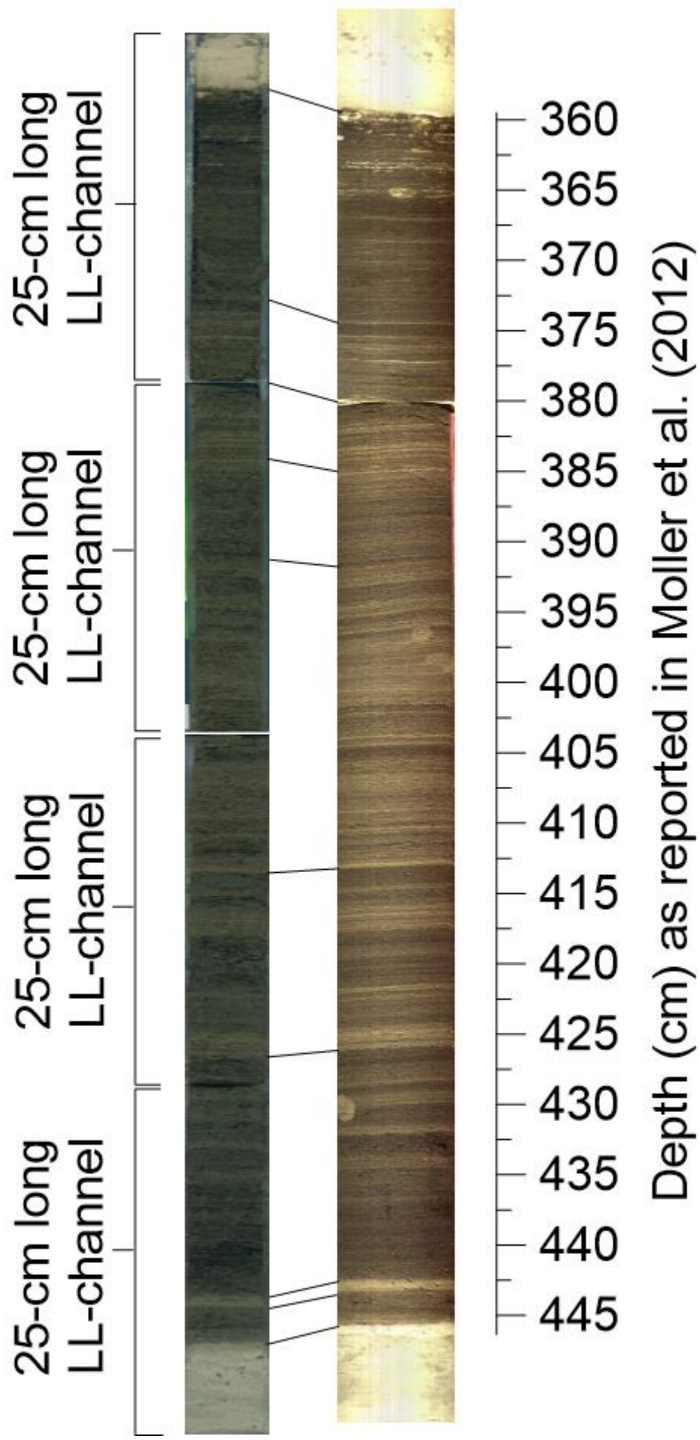

Supplementary Figure 1. Tie-points for adjustment of sampled LL-channels to original depth presented by Moller et al.[6] Due to highly porous nature of the studied sapropel, it expanded a few cm over the years. Here we address this by correlating clearly distinctive layers to adjust expanded sapropel to original depth. Left are line scans of the sampled LL-channels, where right is the initial line scan of the core (Moller, 2012).

The first 3 cm at the onset of the sapropel S5 from M51/3-SL104 core is marked by a stepwise change of colour from a grayish yellow, over dark greenish-gray to olive-gray. The following ~6 cm are built up by alternation of darker (olive-gray to greenish-black) and brighter layers (light olive-gray), ranging between ~5 to 15 mm. In this part, a shift into a diatomic regime at ~9 cm after sapropel onset can be observed. From this point, the coupling of alternating of dark and bright sub-mm lamination (second-order lamination) is indicative of annual layers (varves)[6,9]. One year consists of one bright, almost monospecific lamina and one dark lamina with a more mixed species assemblage[6]. Varve counting was performed by Moller[2] on prepared thin-sections, which were photographed with transmitted light and stitched together to provide a continuous record of the entire S5 sapropel. In total, 2889 laminae couplets consisted of one bright and one dark lamina were counted above ~9cm after sapropel onset.

Since the studied sapropel is highly porous due to the abundance of diatomic frustules, it expanded extend up to a few cm during sample handling and storage. Consequently, although we worked on the same sapropel as Moller[6], around ~1.8 cm expansion in length for the studied sediment core was observed. This was taken into account by correlating 10 clearly visible layers (Supplementary Fig. 1). The recognition of these main marker layers allowed to synchronize the depth and age model with results from previous studies using a linear interpolation between the marker layers.

Reliability of MSI-obtained alkenone-based SST

MSI of sediments is a novel technique in paleoclimate research that provides the possibility to explore molecular proxies with µm-resolution[10–12]. Consequently, obtaining alkenone data with this technique paves the way to explore SST reconstructions with unprecedented temporal resolution. Alkenone-based SST reconstruction has a long tradition in paleoclimate research and represents one of its most reliable tools[1,13,14]. However, most of the alkenone-based SST records are generated in cm-scale resolution (i.e.

multidecadal to multicentennial resolution); thus, the application of this proxy to the reconstruction of sub-decadal to seasonal oscillations is a thrilling challenge.

An evaluation of the suitability of MSI for alkenone-based SST reconstruction was recently performed on varved sediments of the Santa Barbara Basin[15] where they were compared to both conventional molecular proxy analysis and instrumental data. MSI reliably reproduced the instrumental SST time-series for the investigated period. However, on the subannual level reconstructed SST produced a smaller amplitude (12-16°C) compared to actual subannual variability (10-20°C). Considering that in our study the 200 µm resolution in the varved part of sapropel S5 provides rather annual resolution (average varve thickness ~250 µm), we argue that the potential influence of seasonality does not have a great effect on our time-series, particularly that our conclusions are based on the trends from time intervals >30 years. In order to test robustness of the MSI in our study the results were compared to conventional molecular proxy analysis. On a rather coarse resolution, the conventional and the MSI approach showed high consistency in reconstructed SST (Extended Data 3 and 4).

It is also important to consider that alkenone-derived SST reconstructions may be amplified by a physiological response of marine haptophytes to nutrient availability in the surface water. Both culture[16,17] and proxy studies[15] demonstrated positive dependence of the alkenone saturation index to nutrient availability, albeit in a much lesser extent than to SST. Considering that the nutrient enhancement during sapropel formation is related to a significant increase in river run-off, we presume that only SST reconstruction close to the transition from surrounding marl to sapropel is potentially severely influenced by nutrient availability (i.e. the transition from oligotrophic to eutrophic conditions). Since the nutrient flux was rather high but steady during the rest of sapropel S5 deposition, we argue that nutrient concentrations hardly influenced the alkenone-based SST estimates in this part of our record.

Chronological constraints

The timing of the Neogene sapropel deposition in the Mediterranean is related to water column stratification and the consequent establishment of anoxic conditions. This is controlled by precession-obliquity interference that triggers the formation of sapropels due to freshwater input through the African summer monsoon variability, where particularly the precession minima controls northwards migration of the monsoon rain belt over North Africa[18–20]. Consequently, sapropels are used as reliable tie-points in long-term astronomically calibrated timescales for the establishment of robust age models[18,21]. However, establishing precise constraints on the absolute time and duration of sapropel deposition beyond the Holocene is challenging due to limitations in dating of marine sediments and the scarcity of datable volcanic ash layers[8].

This is the case with sapropel S5, where precise direct dating of the sapropel is infeasible. Great progress in improving the absolute chronology of sapropels from the last interglacial-glacial cycle (including sapropel S5) was accomplished by Grant et al.[7]. In their study, they build an age model for the Eastern Mediterranean by correlating high-resolution planktonic foraminiferal $\delta^{18}O$ from core LC21 with the U-Th dated Soreq Cave speleothem $\delta^{18}O$ record[7]. This correlation allowed for the transfer of precisely dated U-Th dated speleothem chronology to core LC21, leading to the establishment of two reliable tie-points for the formation of sapropel S5 at major transitions in $\delta^{18}O$ at onset and end of the sapropel formation. Since the Eastern Mediterranean sapropels can be inter-correlated[22], this allowed for the establishment of reliable absolute chronology of the Last Interglacial Eastern Mediterranean sapropel formation. It is important to note that sapropels deposition should not be strictly synchronous, as their exact timing and duration is related to a number of factors, such as their location in the ocean, local sea level and atmospheric temperature variability[5]. Nevertheless, above explained approach constrained the age for the deposition of sapropel between 121.5-128.3 thousands of years BP (ka)[7,23]. This approach presents a great improvement for the establishment of the sapropel formation on the absolute time scale, however, very precise constraints of the exact duration of sapropel deposition and short-scale changes in sedimentation rates are still unrevealed due to still existing dating uncertainties. For example, 2σ dating uncertainties of approach from Grant et al.[7] are in the range of ±~2 ka from each tie-point, allowing for the large deviation in restraining the duration of sapropel deposition.

Another approach in constraining precise age models is annual layers (varve) counting, when applicable. Although not very useful in establishing an absolute chronology, annual layers counting is a powerful approach for the establishment of precise chronology on a relative time-scale and obtaining the information on short-scale sedimentation rates. Here studied M51/3-SL104 core is varved throughout the major part of the sapropel. An age model for this core was introduced by Moller[2], and it is based on microscopic varve counting and correlation to other sapropels. In short, M51/3-SL104 core was compared against ODP 971A core, as the master core for sapropel S5 stratigraphic correlation[22]. Assuming for similar and continuous accumulation rates of the non-varved part of M51/3-SL104 and comparing it with the corresponding interval of ODP 971A core, it was concluded that lowermost non-varved part of M51/3-SL104 sapropel with a thickness of 9 cm already envelopes ~39% of sapropel deposition duration. The varved (diatomaceous) interval of SL104 sapropel consists of 2889 counted varves[2], depicting the remaining 61% of the total duration. With such temporal constrains, this age model provides an overall age of 4736 years of sapropel formation duration.

The total duration of ~4.8 ka is well comparable with existing results from the literature, although it marks the lower end of published S5 durations[7,24] and it is ~2 ka shorter than duration proposed by Grant et al.[7,23], albeit it is within existing dating uncertainties. We can confidently assume that alternations of bright late spring to late summer lamination with mat-forming diatoms and dark colder season lamination form an annual layer; however, assuming that they are not always regular cannot be ruled out. To test whether the potentially lacking varves on the regular basis would significantly influence the conclusions for this study, we constructed the age model that assumes irregularity of varve deposition by 25% (i.e. assume that each fourth year is missing) to more closely resemble the duration proposed by Grant et al.[7,23] and perform the same rate of decadal SST change and centennial SST change analyses (Supplementary Fig. 2). The results obtained on this alternative approach show fairly comparable amplitude in both decadal and centennial changes when compared to the data on the age model used in our study and consequently support main the conclusions of our study. However, there are no obvious indications that varves deposition is irregular and it is unlikely that there are numerous intervals characterized by large gaps in the varved formations. The only exceptions are three unusually thick laminae of 3-5 mm at the depth between 413-414 cm (coupled dark and bright laminae) and at 433 cm (dark lamina) depth that were related to the duration of one year in existing age model[2]. Despite a potential error, a possible interpolation was abandoned since it is not possible to rule out the possibility of the formation of such an extremely thick lamina during one year. Albeit we suggest interpreting results from those intervals with care, they do not affect the conclusion of this study. Nevertheless, we indicate that the major uncertainty remains in the non-varved part and that results from that part could be strongly dependent on age models applied.

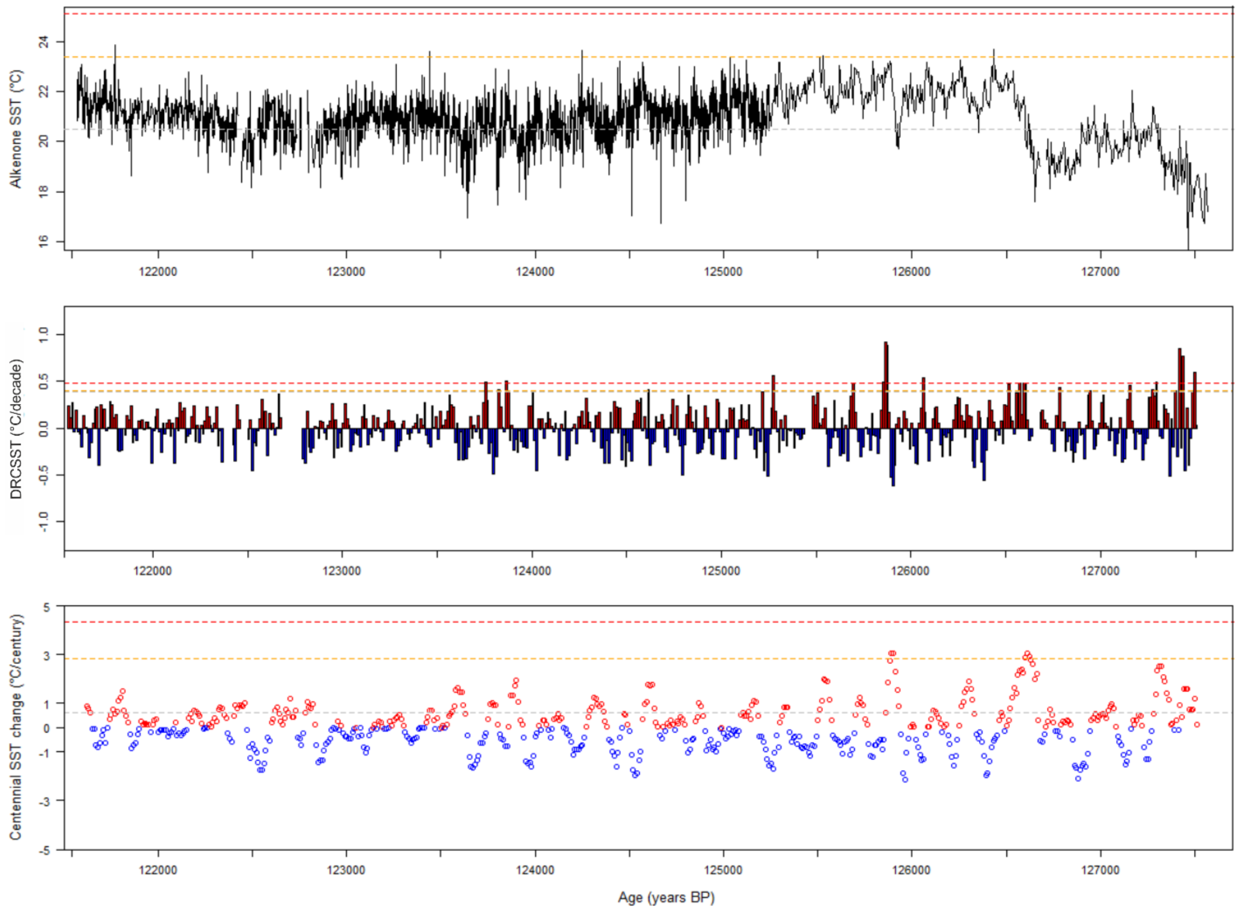

Supplementary Figure 2. Last Interglacial Mediterranean SST on alternative age model, their decadal SST rate of change and centennial SST trends. Same as Fig. 4 in the main manuscript, just with the age model constructed to account for absolute timing indicated by Grant et al.[7]

Supplementary Table 1. CMIP5 and CMIP 6 model simulations used in this study. The set of 31 coupled atmosphere-ocean model runs from the CMIP5 was analysed using the SST fields of the historical simulations covering 1850–2005 AD and the future projections under the RCP4.5 emissions scenario covering 2006-2099 AD. We also analysed the set of 22 model runs from the CMIP6 using the SST fields of the historical simulations covering 1850–2014 AD and the future projections under the SSP-245 and SSP-585 emissions scenarios covering 2015-2099 AD.

	CMIP5	CMIP6
1	ACCESS1-0	ACCESS-CM2
2	ACCESS1-3	ACCESS-ESM1-5
3	bcc-csm1-1	AWI-CM-1-1-MR
4	bcc-csm1-1-m	BCC-CSM2-MR
5	BNU-ESM	CAMS-CSM1-0
6	CanESM2	CanESM5
7	CCSM4	CESM2
8	CESM1-BGC	CIESM
9	CESM1-CAM5	CMCC-ESM2
10	CMCC-CM	EC-Earth3
11	CMCC-CMS	FGOALS-g3
12	CNRM-CM5	FIO-ESM-2-0
13	CSIRO-Mk3-6-0	IITM-ESM
14	FGOALS-g2	INM-CM5-0
15	FIO-ESM	IPSL-CM6A-LR
16	GISS-E2-H	KIOST-ESM
17	GISS-E2-H-CC	MIROC6
18	GISS-E2-R	MPI-ESM1-2-HR
19	GISS-E2-R-CC	MPI-ESM1-2-LR
20	inmcm4	MRI-ESM2-0
21	IPSL-CM5A-LR	NESM3
22	IPSL-CM5A-MR	TaiESM1
23	IPSL-CM5B-LR	
24	NorESM1-M	
25	NorESM1-ME	
26	MIROC5	
27	MIROC-ESM	
28	MIROC-ESM-CHEM	
29	MPI-ESM-LR	
30	MPI-ESM-MR	
31	MRI-CGCM3	

Supplementary references

1. Müller, P. J., Kirst, G., Ruhland, G., von Storch, I. & Rosell-Melé, A. Calibration of the alkenone paleotemperature index U37K’ based on core-tops from the eastern South Atlantic and the global ocean (60°N-60°S). *Geochim. Cosmochim. Acta* **62**, 1757–1772 (1998).
2. Moller, T. F. Formation and paleoclimatic interpretation of a continuously laminated sapropel S5: a window to the climate variability during the Eemian interglacial in the Eastern Mediterranean. (Universität Tübingen, 2012).
3. Marino, G. *et al.* Aegean Sea as driver of hydrographic and ecological changes in the eastern Mediterranean. *Geology* **35**, 675–678 (2007).
4. Rohling, E. J. *et al.* African monsoon variability during the previous interglacial maximum. *Earth Planet. Sci. Lett.* **202**, 61–75 (2002).
5. Dirksen, J. P. & Meijer, P. The mechanism of sapropel formation in the Mediterranean Sea: insight from long-duration box model experiments. *Clim. Past* **16**, 933–952 (2020).
6. Moller, T., Schulz, H., Hamann, Y., Dellwig, O. & Kucera, M. Sedimentology and geochemistry of an exceptionally preserved last interglacial sapropel S5 in the Levantine Basin (Mediterranean Sea). *Mar. Geol.* **291–294**, 34–48 (2012).
7. Grant, K. M. *et al.* Rapid coupling between ice volume and polar temperature over the past 150,000 years. *Nature* **491**, 744–747 (2012).
8. Satow, C. *et al.* Detection and Characterisation of Eemian Marine Tephra Layers within the Sapropel S5 Sediments of the Aegean and Levantine Seas. *Quaternary* **3**, 6 (2020).
9. Kemp, A. E. S., Pearce, R. B., Koizumi, I., Pike, J. & Rance, S. J. The role of mat-forming diatoms in the formation of Mediterranean sapropels. *Nature* **398**, 57–61 (1999).
10. Alfken, S. *et al.* Micrometer scale imaging of sedimentary climate archives – Sample preparation for combined elemental and lipid biomarker analysis. *Org. Geochem.* **127**, 81–91 (2019).

11. Wörmer, L. *et al.* Towards multiproxy, ultra-high resolution molecular stratigraphy: Enabling laser-induced mass spectrometry imaging of diverse molecular biomarkers in sediments. *Org. Geochem.* **127**, 136–145 (2019).

12. Obreht, I. *et al.* An annually resolved record of Western European vegetation response to Younger Dryas cooling. *Quat. Sci. Rev.* **231**, 106198 (2020).

13. Brassell, S. C., Eglinton, G., Marlowe, I. T., Pflaumann, U. & Sarnthein, M. Molecular stratigraphy: a new tool for climatic assessment. *Nature* **320**, 129 (1986).

14. Prahl, F. G. & Wakeham, S. G. Calibration of unsaturation patterns in long-chain ketone compositions for palaeotemperature assessment. *Nature* **330**, 367–369 (1987).

15. Alfken, S. *Refining molecular stratigraphy through mass spectrometry imaging of sediments at sub-millimeter resolution*. (2019).

16. Prahl, F. G., Sparrow, M. A. & Wolfe, G. V. Physiological impacts on alkenone paleothermometry. *Paleoceanography* **18**, (2003).

17. Epstein, B. L., D'Hondt, S., Quinn, J. G., Zhang, J. & Hargraves, P. E. An effect of dissolved nutrient concentrations on alkenone-based temperature estimates. *Paleoceanography* **13**, 122–126 (1998).

18. Hilgen, F. J. Astronomical calibration of Gauss to Matuyama sapropels in the Mediterranean and implication for the Geomagnetic Polarity Time Scale. *Earth Planet. Sci. Lett.* **104**, 226–244 (1991).

19. Lourens, L. J., Wehausen, R. & Brumsack, H. J. Geological constraints on tidal dissipation and dynamical ellipticity of the Earth over the past three million years. *Nature* **409**, 1029–1033 (2001).

20. Rohling, E. J., Marino, G. & Grant, K. M. Mediterranean climate and oceanography, and the periodic development of anoxic events (sapropels). *Earth-Sci. Rev.* **143**, 62–97 (2015).

21. Lourens, L. J. *et al.* Evaluation of the Plio-Pleistocene astronomical timescale. *Paleoceanography* **11**, 391–413 (1996).

22. Cane, T., Rohling, E. J., Kemp, A. E. S., Cooke, S. & Pearce, R. B. High-resolution stratigraphic framework for Mediterranean sapropel S5: defining temporal relationships between records of Eemian climate variability. *Palaeogeogr. Palaeoclimatol. Palaeoecol.* **183**, 87–101 (2002).

23. Grant, K. M. *et al.* The timing of Mediterranean sapropel deposition relative to insolation, sea-level and African monsoon changes. *Quat. Sci. Rev.* **140**, 125–141 (2016).

24. Bar-Matthews, M., Ayalon, A. & Kaufman, A. Timing and hydrological conditions of Sapropel events in the Eastern Mediterranean, as evident from speleothems, Soreq cave, Israel. *Chem. Geol.* **169**, 145–156 (2000).